Projected changes of the warm Arctic-cold North American pattern

Bin Yu[1] and Hai Lin[2]

1. Climate Research Division, Environment and Climate Change Canada, Toronto, Canada

2. Meteorological Research Division, Environment and Climate Change Canada, Dorval, Canada

Corresponding author address:

Bin Yu, Climate Research Division, Environment and Climate Change Canada, 4905 Dufferin Street, Toronto, ON M3H 5T4. Email: bin.yu@ec.gc.ca

Key points:

• WACNA variability decreases with global warming, with a faster decline in the Chukchi-Bering Seas than North America

• WACNA variability is mainly generated by meridional heat transport and damped by the covariance between temperature and diabatic heating

• WACNA changes are driven by alternations in meridional heat transport, related to global warming and its featured Arctic amplification

Abstract

The Warm Arctic - Cold North American (WACNA) pattern features opposing surface temperature anomalies, with centers over the Chukchi - Bering Seas (CBS) and the North American Great Plains. This pattern is found to be driven and sustained by meridional heat transport along temperature gradients, primarily damped by the covariance between temperature and diabatic heating. The Canadian Earth System Model CanESM5, part of the Coupled Model Intercomparison Project Phase 6 (CMIP6), reasonably reproduces this pattern and its formation mechanisms. CanESM5 projections under the Shared Socioeconomic Pathway 8.5 (SSP5-8.5) suggest a significant weakening of the WACNA pattern with continued global warming. Notable changes in pattern intensity and spatial structure are anticipated, particularly a decrease in intensity over the CBS. These changes are attributed to Arctic amplification associated with global warming, which diminishes the equator-to-pole temperature gradient and consequently reduces meridional heat transport, particularly over the CBS region.

Plain Language Summary

The Warm Arctic - Cold North American (WACNA) pattern shows warming in the Arctic and cooling in North America, with hot spots in the Chukchi - Bering Seas (CBS) and the Great Plains. This happens because heat moves from one place to another along temperature differences, balanced mainly by the interaction of temperature and diabatic heating. We explore how global warming affects this pattern using the latest Canadian Earth System Model CanESM5. The model does a good job of simulating this pattern and why it happens. According to CanESM5's simulations under a future scenario called SSP5-8.5, the WACNA pattern will become weaker as the Earth keeps warming up, especially over the CBS. These changes are due to a phenomenon called Arctic amplification, where warming happens faster in the Arctic than in other places. This reduces the movement of heat from the equator to the Arctic, especially in the CBS region, causing changes in the WACNA pattern.

Key words: WACNA, Impact of climate change, Maintenance mechanism

1. Introduction

Recent studies have actively delved into the warm Arctic – cold continents pattern (WACC, Overland et al. 2011), particularly investigating its distinct features, climate impacts, and formation mechanisms. This pattern is characterized by Arctic warming and continental cooling during boreal winter and manifests in two counterparts corresponding to midlatitude climate anomalies: warm Arctic-cold Eurasia (WACE; e.g., Cohen et al. 2012; Mori et al. 2014, 2019; Sorokina et al. 2016) and warm Arctic-cold North America (WACNA; e.g., Lin, 2015; Blackport et al., 2019; Guan et al., 2020a; Yu and Lin, 2022; Lin et al., 2022). The genesis of the WACNA pattern is attributed to both external forcing and internal climate variability, such as Eurasian snow cover and Chukchi-Bering Sea sea ice anomalies (e.g., Lin and Wu, 2011; Cohen et al., 2012; Kug et al., 2015; Park et al., 2021), tropical convection and El Niño-Southern Oscillation (ENSO) sea surface temperature (SST) anomalies (Lin, 2015; Guan et al., 2020a; Yu and Lin, 2022), and atmospheric circulation anomalies (Sun et al., 2016; Sigmond and Fyfe, 2016; Blackport et al., 2019; Guan et al., 2020b; Yu and Lin, 2022; Lin et al., 2022). These studies have significantly enriched our understanding of Arctic atmospheric circulation anomalies and their interconnections with other regions, offering potential for improving seasonal forecasts in northern midlatitudes.

Anthropogenic global warming is marked by well-established features including Arctic circulation anomalies, Arctic amplification, and tropical ENSO-like SST anomalies (e.g., Cohen et al., 2020; IPCC, 2021), all closely linked to the formation of WACNA. Consequently, this study is dedicated to exploring the future evolution and underlying mechanisms of the WACNA pattern. The questions guiding our investigation are as follows: 1) How is the WACNA pattern expected to change with global warming? Are changes anticipated in its intensity and/or spatial structure?

2) What are the physical mechanisms driving the WACNA variability in terms of the temperature variance budget? How do these mechanisms evolve in response to global warming?

2. Data and Methodology

2.1 Reanalysis data and climate simulations

Atmospheric variables extracted from the fifth generation of atmospheric reanalysis (ERA5, Hersbach et al., 2020), developed by the European Centre for Medium-Range Weather Forecasts (ECMWF), are employed as observations. The variables we used include surface air temperature (SAT) as well as lower tropospheric temperature and winds. These variables are analyzed on 2.5° × 2.5° grids over the period from 1981 to 2010, consistent with the later period of historical climate simulations described below. Years refer to January dates in this study.

Outputs from CanESM5 climate simulations are also utilized. CanESM5 has a horizontal T63 spectral resolution of approximately 2.8° in the atmosphere and 1° in the ocean (Swart et al., 2019). Detailed description of the model can be found on the website CanESM5 - The Canadian Earth System Model version 5 - Open by Default Portal (canada.ca). Our analysis focuses on its Single Model Initial-condition Large Ensemble (SMILE), which includes historical and scenario climate simulations. The ensemble consists of 50 members with 251-year integrations spanning from 1850 to 2100. Each simulation is subject to the same historical anthropogenic and natural forcing from 1850 to 2014, but with slightly different initial conditions in 1850, and multiple Shared Socioeconomic Pathway (SSP) scenarios for climate change simulations for 2015–2100. Here, we use simulations under the SSP5-8.5 scenario, representing high anthropogenic emissions (Eyring et al., 2016). The extracted variables also include monthly SAT, and temperature and winds in the lower troposphere. These variables are interpolated to 2.5° × 2.5° grids using bilinear interpolation.

2.2 Data processing and statistical analysis

To focus on intraseasonal to interannual variability, monthly anomalies are considered as 10-year high-pass filtered fluctuations of variables. The result is insensitive to reasonable variation of the filter cutoff period. The WACNA pattern is then defined as the leading mode of monthly SAT anomalies in winter (December-February, DJF) over the North American (NA) sector (e.g., Yu and Lin, 2022), removing the climatology of the period considered. The corresponding principal component (PC1) is used as an index of the WACNA pattern. EOF analysis is also performed to capture the WACNA pattern simulated by CanESM5, using 50 ensemble simulations as a collective dataset. The multi-member ensemble mean (EnM) quantity is obtained by pooling the statistics of individual members, i.e. the average of the 50 member results. The impact of internal climate variability on WACNA is assessed by examining inter-member variations of simulated WACNA patterns. Individual WACNA patterns are obtained by regressing SAT anomalies onto the corresponding PC1 series among the 50 members. Correlation and regression analyses are used to quantify relationships between the WACNA index and variables of interest. The statistical significance of a correlation is determined by a Student-t test, with the effective degree of freedom estimated by considering the autocorrelation of the time series (Bretherton et al., 1999). To avoid potential over-interpretation of multiple testing results for grid points over a domain of interest, we apply the false detection rate (FDR) approach demonstrated in Wilks (2016) as a field significance test.

2.3 Temperature variance equation

The thermodynamic energy equation can be written as follows

$$\frac{dT}{dt} = \omega\kappa\frac{T}{p} + \frac{Q}{C_p}, \qquad (1)$$

where T is temperature, t time, p pressure, $\omega=dp/dt$ the vertical velocity in pressure coordinates, $\kappa=R_d/C_p$, where R_d is the gas constant for dry air, C_p the specific heat at constant pressure, and Q the net heating rate per unit mass. Q includes various diabatic effects, including radiative (solar and infrared) heating, turbulent (latent and sensible) heating, and frictional heating. Expanding the total derivative of temperature, we have

$$\frac{\partial T}{\partial t} = -\left(u\frac{\partial T}{\partial x} + v\frac{\partial T}{\partial y}\right) + \omega\left(\kappa\frac{T}{p} - \frac{\partial T}{\partial p}\right) + \frac{Q}{C_p} \equiv -u\frac{\partial T}{\partial x} - v\frac{\partial T}{\partial y} + S + R, \quad (2)$$

where u and v are the zonal and meridional wind speeds, respectively. $S=\omega\left(\kappa\frac{T}{p} - \frac{\partial T}{\partial p}\right)$ is a vertical motion term containing the static stability (e.g., Peixoto and Oort, 1992), and $R=Q/C_p$ is considered as a residual in the equation. Based on Eq. (2), the associated temperature variance equation can be written as

$$\frac{1}{2}\frac{\partial \overline{T'^2}}{\partial t} = -\overline{u'T'}\frac{\partial \bar{T}}{\partial x} - \frac{\bar{u}}{2}\frac{\partial \overline{T'^2}}{\partial x} - \overline{\frac{u'}{2}\frac{\partial T'^2}{\partial x}} - \overline{v'T'}\frac{\partial \bar{T}}{\partial y} - \frac{\bar{v}}{2}\frac{\partial \overline{T'^2}}{\partial y} - \overline{\frac{v'}{2}\frac{\partial T'^2}{\partial y}} + \overline{T'S'} + \overline{T'R'}$$

$$\equiv UT1 + UT2 + UT3 + VT1 + VT2 + VT3 + TS + TR, \quad (3)$$

where the prime denotes monthly anomalies relative to the climatology. The overbar represents the time average over the period considered. Eq. (3) shows that the temperature variance tendency depends on eight factors: $UT1=-\overline{u'T'}\frac{\partial \bar{T}}{\partial x}$ is the zonal heat transport along the temperature gradient, $UT2=-\frac{\bar{u}}{2}\frac{\partial \overline{T'^2}}{\partial x}$ and $UT3=-\overline{\frac{u'}{2}\frac{\partial T'^2}{\partial x}}$ the zonal advection of temperature variance caused by zonal mean and anomalous flows, respectively, $VT1=-\overline{v'T'}\frac{\partial \bar{T}}{\partial y}$ the meridional heat transport along the temperature gradient, $VT2=-\frac{\bar{v}}{2}\frac{\partial \overline{T'^2}}{\partial y}$ and $VT3=-\overline{\frac{v'}{2}\frac{\partial T'^2}{\partial y}}$ the meridional advection of temperature variance caused by meridional mean and anomalous flows, respectively, TS the covariance between temperature and effects related to vertical motion and static stability, and TR the covariance between temperature and diabatic heating, which is calculated as a residual. These terms act to generate or damp temperature variances, depending on their signs. The anomalous temperature square ($\overline{T'^2}$) is proportional to the available potential energy (e.g., Lorenz, 1955) and is also called the thermal variance (Lin and Derome, 1995).

As discussed below, *VT1* is an important term that causes changes in temperature variability. Changes in *VT1* can be further decomposed into three subcomponents as follows,

$$\delta(VT1) = -\overline{v'T'}_0\delta\left(\frac{\partial \bar{T}}{\partial y}\right) - \left(\frac{\partial \bar{T}}{\partial y}\right)_0 \delta(\overline{v'T'}) - \delta(\overline{v'T'})\cdot\delta\left(\frac{\partial \bar{T}}{\partial y}\right) \equiv VT1a + VT1b + VT1c\,, \quad (4)$$

where the delta denotes the change between two periods considered, and the subscript 0 denotes the initial period. The three terms on the right side of the equation represent contributions of changes in the mean temperature [$VT1a = -\overline{v'T'}_0\delta\left(\frac{\partial \bar{T}}{\partial y}\right)$], the meridional heat transport [$VT1b = -\left(\frac{\partial \bar{T}}{\partial y}\right)_0 \delta\left(\overline{v'T'}\right)$], and both [$VT1c = -\delta(\overline{v'T'})\cdot\delta\left(\frac{\partial \bar{T}}{\partial y}\right)$].

3. Results

3.1 Changes in WACNA pattern intensity and spatial structure

Figure 1 (left panels) displays the WACNA patterns in both ERA5 and CanESM5 simulations. These patterns are identified as the leading mode (EOF1) of monthly SAT anomalies over the NA sector (20-90^{o}N, 150^{o}E-40^{o}W) during the 30 DJFs from 1981-2010. In ERA5 (Fig.1, top left), EOF1 accounts for 32.8% of the total variance and is well separated from subsequent EOFs based on the criterion of North et al. (1982). It is characterized by a dipole structure, which features a pronounced SAT anomaly over NA, centered on the Great Plains, accompanied by an opposing anomaly spreading across the central-eastern Arctic and mid-high latitude North Pacific, centered on the Chukchi-Bering Seas (CBS). This pattern closely resembles WACNA patterns identified across intraseasonal and interannual timescales in various observational datasets (e.g., Kug et al., 2015; Lin, 2015; Guan et al., 2020a; Yu and Lin, 2022, 2023; Lin et al., 2022), highlighting its robustness and consistence among different time scales. In CanESM5, EOF analysis is conducted using the same 30 DJFs from all 50 historical simulations. The simulated EOF1 (Fig. 1, bottom left) explains 29.6% of the total SAT variance and closely resembles the ERA5 result, with a pattern correlation of 0.91 over the NA sector, indicating that WACNA is reasonably well reproduced by CanESM5. Nevertheless, in CanESM5, the action centers of WACNA appear slightly stronger compared to ERA5, especially the CBS center, and are slightly shifted eastward.

To quantitatively evaluate changes in WACNA, we project SAT anomalies over 30-DJF running windows for 1951-2014 from historical simulations and 2015-2100 from SSP5-8.5 simulations onto the simulated WACNA pattern over the NA sector (Fig. 1, bottom left). The amplitude of WACNA variability is then assessed by calculating the standard deviation for each projected 30-DJF series (Fig. 1, right). Notably, the ensemble mean of WACNA amplitude decreases with global warming, especially under the SSP forcing after 2015, with variability decreasing by approximately 40% from 1951-1980 (1.05) to 2071-2100 (0.64). To further explore changes in the spatial structure of WACNA, similar projections are conducted over the two action centers in CBS and NA. The results obtained are not sensitive to a slight change of the projected domains. Interestingly, CBS variability exhibits a marked reduction of about 70% from 1951-1980 (1.4) to 2071-2100 (0.45), contrasting with a modest decrease of approximately 20% in NA variability from 1.0 to 0.81. Additionally, we examine the ensemble spread among 50 members (Fig. 1, right). The relative contributions of external forcing and internal variability can be quantified by the signal-to-noise ratio (SNR) of the EnM to the inter-member standard deviation. Most changes have SNRs above 10 (not shown), indicating substantial forced changes compared to internal variability.

Changes in the intensity and spatial structure of the WACNA pattern are also readily discernible when comparing the patterns for 1951-1980 and 2071-2100 (Fig. 2, left panels). Here, we show the temperature anomalies at 925-hPa (T_{925}) associated with WACNA, which closely resemble surface anomalies (not shown). The dipole structure appears in both periods, but is markedly asymmetric in the later period, with a strong center at NA and a weak center at CBS. Contrasting the T_{925} regressions for 2071-2100 with those for 1951-1980 reveals negative values over CBS and positive values over NA (Fig. 2, top right), indicating that both centers are declining in strength with global warming. However, the maximum temperature anomaly at the CBS center drops from 2.8^{o}C in 1951-1980 to 1.3^{o}C in 2071-2100, which is faster than the increase in NA from -3.8^{o}C to -3.1^{o}C. Meanwhile, both centers exhibit a slightly westward shift in 2071-2100 relative to 1951-1980. The diminishing trend of strength in both centers with global warming can be seen more clearly when comparing the difference of T_{925} regression squares between the two periods (Fig. 2, bottom right), indicating a change in the temperature variance associated with WACNA. The regional mean temperature variance in CBS (57.5-75^{o}N, 175^{o}E-150^{o}W) drops from 4.5^{o}C^{2} in 1951-1980 to 0.7^{o}C^{2} in 2071-2100, which is faster than the decrease in NA (45-65^{o}N, 120-75^{o}W) from 7.5^{o}C^{2} to 3.4^{o}C^{2}.

Overall, WACNA variability decreases with global warming, with a faster decline in the CBS center compared to North America.

3.2 WACNA variability and change mechanisms

We investigate the physical mechanisms of WACNA variability in terms of the temperature variance budget given in Eq. (3). The temperature variance budget quantities at 925-hPa associated with WACNA are calculated for the period 1981-2010 in both ERA5 and CanESM5. The WACNA variability is mainly generated and maintained by the meridional heat transport along the temperature gradient (*VT1*) and damped by the covariance between temperature and diabatic heating (*TR*), as depicted in Figs. S1 and S2. Additionally, the covariance between temperature and factors related to vertical motion and static stability (*TS*) also contributes to the WACNA variability, together with relatively weak effects from the zonal heat transport along the temperature gradient (*UT1*) and the zonal and meridional advections of temperature variance (*UT23=UT2+UT3* and *VT23=VT2+VT3,* the advections caused by both mean and anomalous flows are weak) over North America. These contributions exhibit similar features in ERA5 and CanESM5, indicating that CanESM5 reasonably well captures the observed WACNA variability mechanisms. However, the contribution patterns appear smoother in CanESM5 compared to ERA5 (Figs. S1 and S2), partly due to the large amount of pooled data used in the CanESM5 calculation.

Figure 3 further compares the three dominant temperature variance budget terms in ERA5 and CanESM5. *VT1* is responsible for amplifying the WACNA variability, showing high values over CBS and NA corresponding to the main WACNA action centers (Fig. 2), in contrast to damping effects dominated by *TR*. *TS* exhibits positive effects over the Chukchi Sea and central-western Canada, but negative effects over the Bering Sea and along the western coast of Canada. These three contributions demonstrate broad comparability between ERA5 and CanESM5, except for intensity differences in CBS. Notably, the quantities of *VT1* and *TR* in the CBS region are approximately 20-30% stronger in CanESM5 compared to ERA5. This may also be the reason why the action center of simulated WACNA in CBS is stronger (Fig. 1).

The changes in temperature variance budget quantities at 925-hPa from the period 1951-1980 to 2071-2100 are displayed in Fig. 4. Changes in WACNA variability are a consequence of all processes taking place in the simulated climate change and are dominated by changes in *VT1*, *TR* and *TS*, as well as relatively weak adjustments in *UT23*, *VT23* and *UT1* observed in North America.

Negative *VT1* values over CBS and NA (Fig. 4) indicate a decline in meridional heat transport along the temperature gradient, which acts to support the decrease in WACNA-associated temperature variance (Fig. 2, bottom right). The reduction of *VT1* in CBS is stronger than that in NA, which may explain the larger decrease of amplitude in the CBS center of WACNA than NA as seen in Fig. 2. Changes in *VT1* are mainly balanced by changes in *TR* and *TS*. Furthermore, the changes in *VT1* are primarily influenced by the changes in the mean temperature term (*VT1a*), whose magnitude is approximately two to three times larger than the *VT1b* and *VT1c* terms (Fig. S3). Hence, these changes are closely related to global warming and its featured Arctic amplification (e.g., Francis et al., 2017; Cohen et al., 2020; IPCC, 2021). As global warming advances, Arctic amplification reduces the equator-to-pole temperature gradient, resulting in lower *VT1a* and *VT1* according to Eq. (4).

Figure 5 provides additional insights into the time evolution of WACNA-associated temperature variance budget changes in CBS and NA by showing the regional mean changes in the three dominant budget terms and the three *VT1* subcomponents from 1951 to 2100. The evolution reveals stable changes, especially significant trends under the SSP forcing after 2015. In addition, the change in the regional mean quantities is stronger in CBS than in NA, as seen in Fig. 4. The evolution results again highlight the importance of reductions in *VT1* and its subcomponent *VT1a* in organizing and maintaining the decrease of WACNA variability in both centers against damping effects dominated by *TR*.

4. Summary and discussion

This study explores the future changes and underlying mechanisms of the WACNA pattern, using data from the ERA5 reanalysis and 50 ensemble members of CanESM5 simulations under historical and SSP5-8.5 scenarios. CanESM5 reasonably reproduces the WACNA pattern and its temperature variance budget mechanisms, consistent with ERA5 results.

WACNA variability decreases with global warming, particularly in the Chukchi-Bering Sea region and at a faster rate than in North America. The variability of WACNA is mainly driven and maintained by meridional heat transport along temperature gradients, balanced by the covariance between temperature and diabatic heating. Additionally, factors related to vertical motion and static stability contribute modestly to WACNA variability. Changes in WACNA variability also arise from alternations in meridional heat transport, primarily influenced by changes in mean temperatures, with damping effects largely driven by changes in the covariance between temperature and diabatic heating. Consequently, changes in WACNA variability are closely related to global warming and its featured Arctic amplification, which reduces the equator-to-pole temperature gradient, leading to decreased meridional heat transport.

The findings regarding changes in the strength and spatial structure of the WACNA pattern, along with the WACNA variability and change mechanisms, deepen our understanding of the Arctic-midlatitude relationship. They also shed light on how global warming impacts internal climate variability, particularly the connection between Arctic amplification and midlatitude climate variability. Given that CanESM5 exhibits higher climate sensitivity compared to many CMIP6 models (Meehl et al., 2020; Sherwood et al., 2020), however, uncertainties in WACNA simulations due to factors like model parameterizations and structural differences remain to be addressed. In addition, it would be intriguing to investigate whether similar changes and mechanisms apply to the WACE pattern over Eurasia.

Acknowledgements: We thank the work of colleagues at the CCCma in the production of the CanESM5 simulations analyzed here. The ERA5 reanalysis data was downloaded from the website: https://cds.climate.copernicus.eu/cdsapp#!/search?type=dataset.

Data availability: Data and analysis methods used in this study are described in Section 2.

References

Blackport, R., J.A. Screen, K. van der Wiel, and R. Bintanja, 2019: Minimal influence of reduced Arctic sea ice on coincident cold winters in mid-latitudes. *Nat. Clim. Change*, **9**, 697–704.

Bretherton, C.S., M. Widmann, V.P. Dymnikov, J.M. Wallace, and I. Bladé, 1999: The effective number of spatial degrees of freedom of a time-varying field. *J. Clim.*, **12**, 1990-2009.

Cohen, J., J. C. Furtado, M. Barlow, V. Alexeev, and J. Cherry, 2012: Arctic warming, increasing snow cover and widespread boreal winter cooling. *Env. Res. Lett.*, **7**, 014007.

Cohen, J., X. Zhang, J. Francis, and co-authors, 2020: Divergent consensuses on Arctic amplification influence on midlatitude severe winter weather. *Nat. Clim. Chang.* **10**, 20-29.

Eyring, V., and co-authors, 2016: Overview of the Coupled Model Intercomparison Project Phase 6 (CMIP6) experimental design and organization. *Geosci. Model Dev*., **9**, 1937-1958.

Francis, J. A., and S. J. Vavrus, 2012: Evidence linking Arctic amplification to extreme weather in mid-latitudes. *Geophys. Res. Lett.*, **39**, L06801.

Guan, W., X. Jiang, X. Ren, G. Chen, P. Lin, and H. Lin, 2020a: The Leading Intraseasonal Variability Mode of Wintertime Surface Air Temperature over the North American Sector. *J. Clim*., **33**, 9287-9306.

Guan, W., X. Jiang, X. Ren, G. Chen, and Q. Ding, 2020b: Role of atmospheric variability in driving the “warm-Arctic, cold continent” pattern over the North America sector and sea ice variability over the Chukchi-Bering Sea. *Geophys. Res. Lett.*, **47**, e2020GL088599.

Hersbach, H. and co-authors, 2020: The ERA5 global reanalysis. *Q. J. R. Meteorol. Soc.*, **146**, 1999-2049.

IPCC, 2021: *Climate Change 2021: The Physical Science Basis*. Cambridge University Press, Cambridge, 2391 pp, doi:10.1017/9781009157896.

Kug, J.S., and co-authors, 2015: Two distinct influences of Arctic warming on cold winters over North America and East Asia. *Nat. Geos.*, **8**, 759-762.

Lin, H., 2015: Subseasonal variability of North American wintertime surface air temperature. *Clim. Dyn.*, **45**, 1137–1155.

Lin, H., and J. Derome, 1995: On the thermal interaction between the synoptic-scale eddies and the intraseasonal fluctuations in the atmosphere, *Atmos-Ocean*, **33**, 81-107.

Lin, H., and Z.W. Wu, 2011: Contribution of the autumn Tibetan Plateau snow cover to seasonal prediction of North American winter temperature. *J. Clim.*, **24**, 2801–2813.

Lin, H., B. Yu, and N.M.J. Hall, 2022: Origin of the warm Arctic – cold North American pattern on the intraseasonal time scale. *J. Atmos. Sci.*, **79**, 2571-2583.

Lorenz, E.N., 1955: Available potential energy and the maintenance of the general circulation. *Tellus*, **7**, 157–167.

Meehl, G.A., and co-authors, 2020: Context for interpreting equilibrium climate sensitivity and transient climate response from the CMIP6 Earth system models. *Sci. Adv.*, **6**, eaba1981, doi: 10.1126/sciadv.aba1981.

Mori, M., Y. Kosaka, M. Watanabe, H. Nakamura, and M. Kimoto, 2019: A reconciled estimate of the influence of Arctic sea-ice loss on recent Eurasian cooling. *Nat. Clim. Change*, **9**, 123-129.

Mori, M., M. Watanabe, H. Shiogama, J. Inoue, and M. Kimoto, 2014: Robust Arctic sea-ice influence on the frequent Eurasian cold winters in past decades. *Nat. Geos.*, **7**, 869–873.

North, G.R., T.L. Bell, R.F. Cahalan, and F.J. Moeng, 1982: Sampling errors in the estimation of empirical orthogonal functions. *Mon. Wea. Rev.*, **110**, 699–706.

Overland, J. E., K.R. Wood, and M. Wang, 2011: Warm Arctic - Cold continents: Climate impacts of the newly open Arctic sea. *Polar Res.*, **30**, 15787.

Park, H.L., and co-authors, 2021: Dominant wintertime surface air temperature modes in the Northern Hemisphere extratropic. *Clim. Dyn*., **56**, 687–698.

Peixoto, J., and A. Oort, 1992: The physics of climate, AIP, NY, 520pp.

Sherwood, S., and co-authors, 2020: An assessment of Earth's climate sensitivity using multiple lines of evidence. *Rev. Geophys*., doi: 10.1029/2019RG000678.

Sigmond, M., and J.C. Fyfe, 2016: Tropical Pacific impacts on cooling North American winters. *Nat. Clim. Change*, **6**, 970–974.

Sorokina, S.A., C. Li, J.J. Wettstein, and N.G. Kvamstø, 2016: Observed atmospheric coupling between Barents Sea ice and the warm-Arctic cold-Siberian anomaly pattern. *J. Clim.* **29**, 495-511.

Sun, L.T., J. Perlwitz, and M. Hoerling, 2016: What caused the recent "warm Arctic, cold continents" trend pattern in winter temperatures? *Geophys. Res. Lett.*, **43**, 5345-5352.

Swart, N.C., and co-authors, 2019: The Canadian Earth System Model version 5 (CanESM5.0.3). *Geosci. Model Dev*., **12**, 4823-4873.

Wilks, D. S., 2016: “The stippling shows statistically significant grid points”: How research results are routinely overstated and overinterpolated, and what to do about it. *Bull. Amer. Meteor. Soc.*, **97**, 2263–2273.

Yu, B., and H. Lin, 2022: Interannual variability of the warm Arctic - cold North American pattern. *J. Clim.*, **35**, 4277-4290.

Yu, B., and H. Lin, 2023: The warm Arctic-cold North American pattern in CanESM5 large ensemble simulations: Eurasian influence and uncertainty due to internal variability. *Clim. Dyn.*, doi: 10.1007/s00382-023-06966-6.

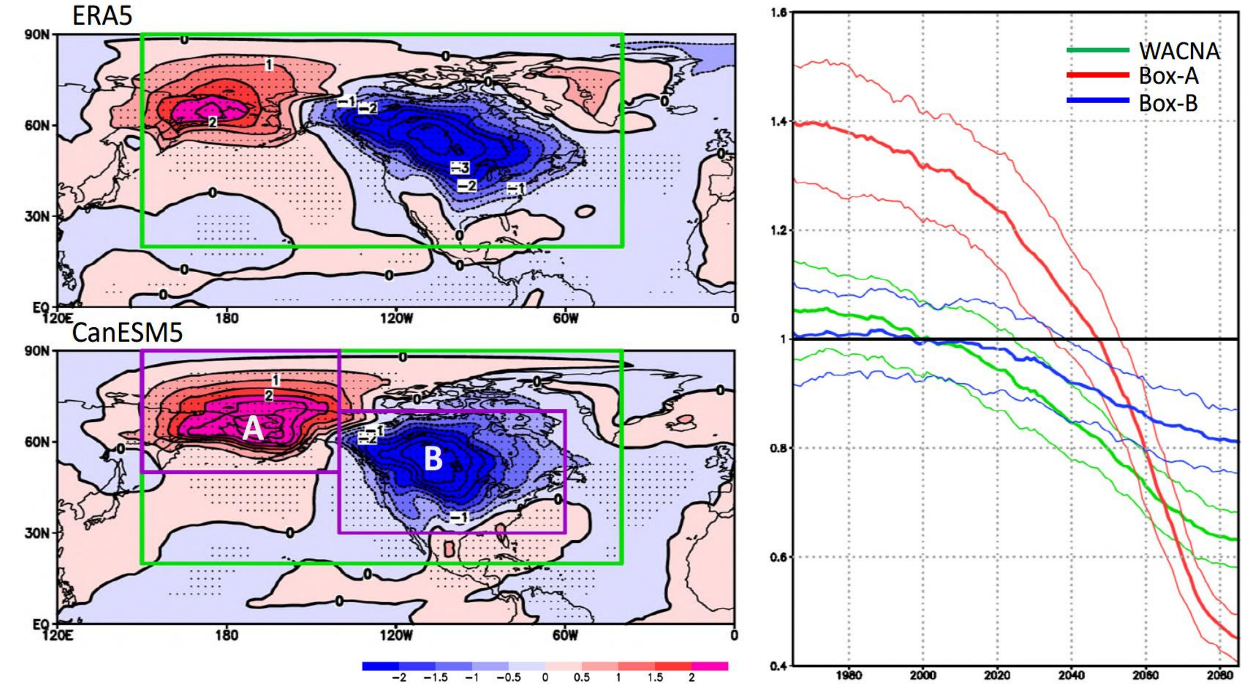

Figure 1 (left) Regressions of SAT anomalies onto the WACNA index over 1981-2010 for the ERA5 reanalysis (top) and CanESM5 EnM (bottom). The green box indicates the region of (20-90^{o}N, 150^{o}E-40^{o}W) used for the EOF analysis to define the WACNA pattern. The purple boxes A and B indicate the regions of (50-90^{o}N, 150^{o}E-140^{o}W) over CBS and (30-70^{o}N, 140-60^{o}W) over NA, respectively. Contour interval is 0.5^{o}C. Black dots indicate the regression is statistically significant with p values small enough to satisfy the FDR criterion of $\alpha_{FDR} = 0.05$. (right) Changes in amplitude of WACNA variability for 1951-2014 from historical simulations and for 2015-2100 from SSP simulations. The amplitude of WACNA variability is defined as the standard deviation of the SAT anomalies projected onto the WACNA pattern within the WACNA domain (green), Box-A (red), and Box-B (blue) over 30-year running windows. EnM is represented by the thick curve. Ensemble spread, indicated by EnM plus and minus one inter-member standard deviation for 50 results, is shown by thin curves. Years are labeled based on year 15 of a 30-year window.

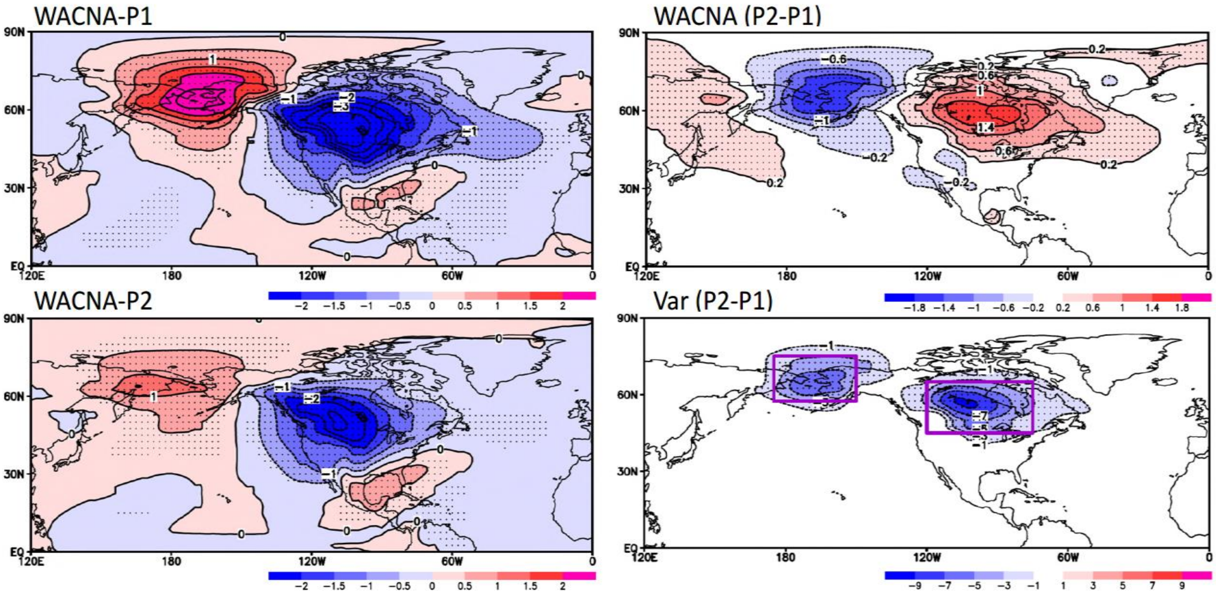

Figure 2 (left) Regression of T_{925} anomalies onto the WACNA index over 1951-1980 (top) and 2071-2100 (bottom) for the CanESM5 EnM. Contour interval is 0.5°C. Black dots indicate the regression is statistically significant with p values small enough to satisfy the FDR criterion of $\alpha_{FDR} = 0.05$. (right) Difference (top) and squared difference (bottom) between T_{925} regressions for 2071-2100 and 1951-1980. Contour intervals are 0.4°C (…, -0.6, -0.2, 0.2, 0.6, …) for the difference and 2.0°C^2 (…, -3, -1, 1, 3, …) for the square difference. Black dots indicate significant differences with a value greater than 0.2 °C for the difference (1.0 °C^2 for the square difference) and a 95% confidence level. The two purple boxes indicate the regions of (57.5-75°N, 175°E-150°W) in CBS and (45-65°N, 120-75°W) in NA used for the temperature variance diagnostic.

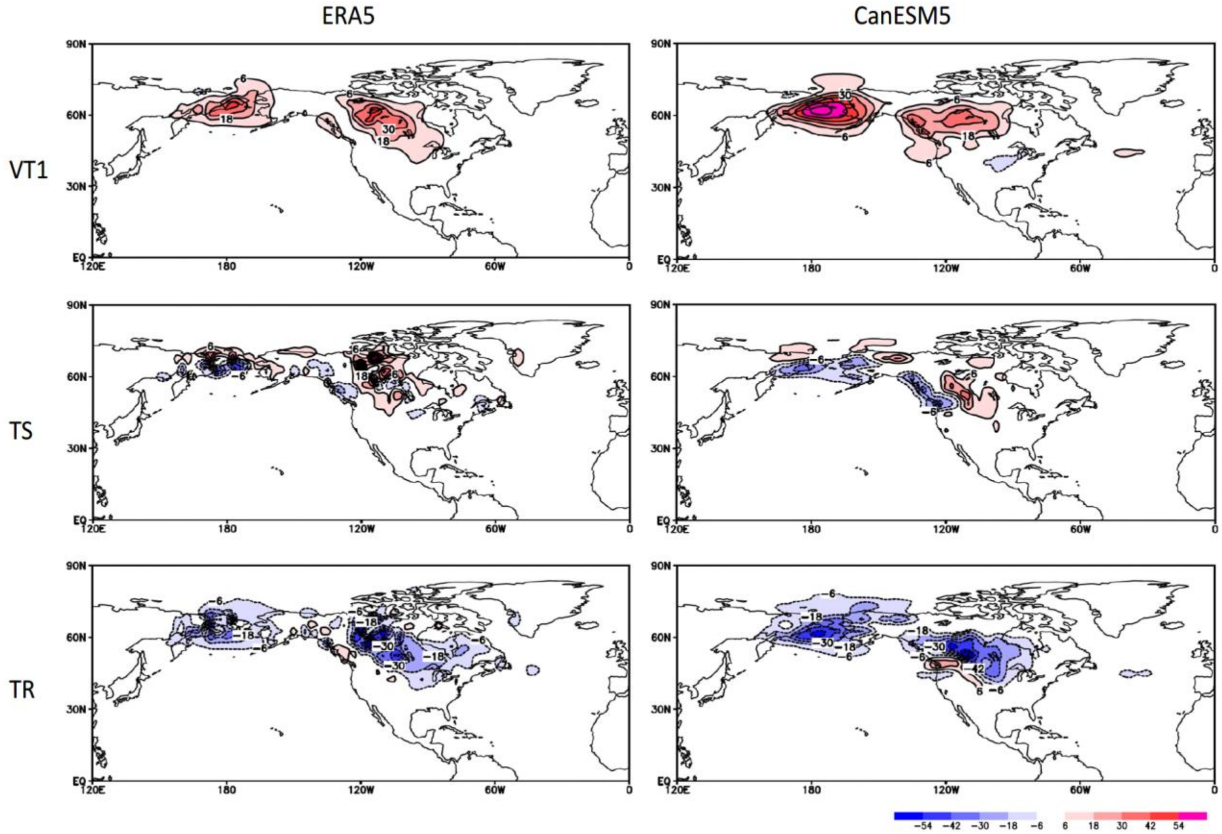

Figure 3 VT1 (top), TS (middle), and TR (bottom) anomalies at 925-hPa associated with the WACNA index over 1981-2010 for the ERA5 reanalysis (left) and CanESM5 EnM (right). Contour interval is 12 $\times 10^{-6}\,{}^{o}C^2s^{-1}$ (…, -18, -6, 6, 18, …).

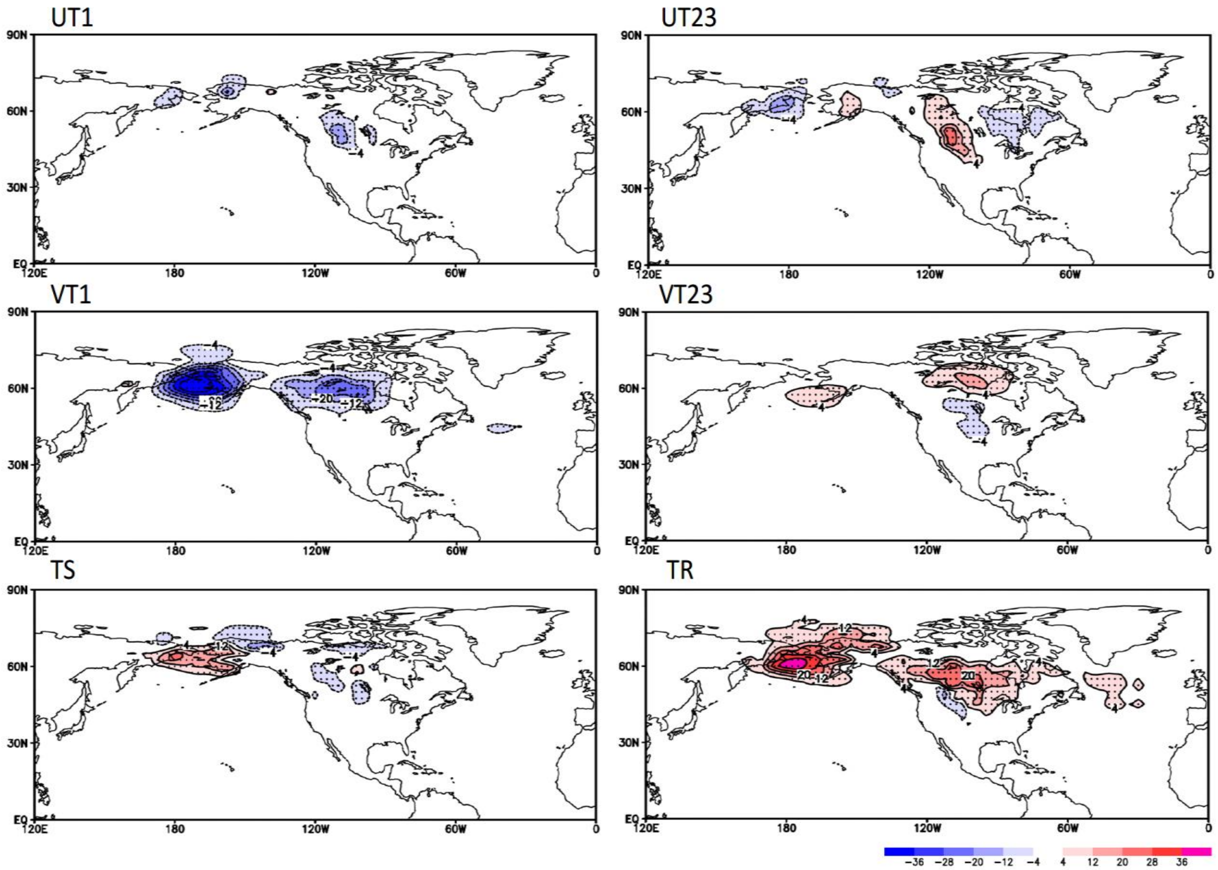

Figure 4 Changes of UT1, UT23, VT1, VT23, TS, and TR anomalies at 925-hPa associated with the WACNA index from 1951-1980 to 2071-2100 for the CanESM5 EnM. Contour interval is 8 x10^{-6} $^{o}C^{2}s^{-1}$ (…, -12, -4, 4, 12, …). Black dots indicate significant differences with a difference value greater than 4 x10^{-6} $^{o}C^{2}s^{-1}$ and a 95% confidence level.

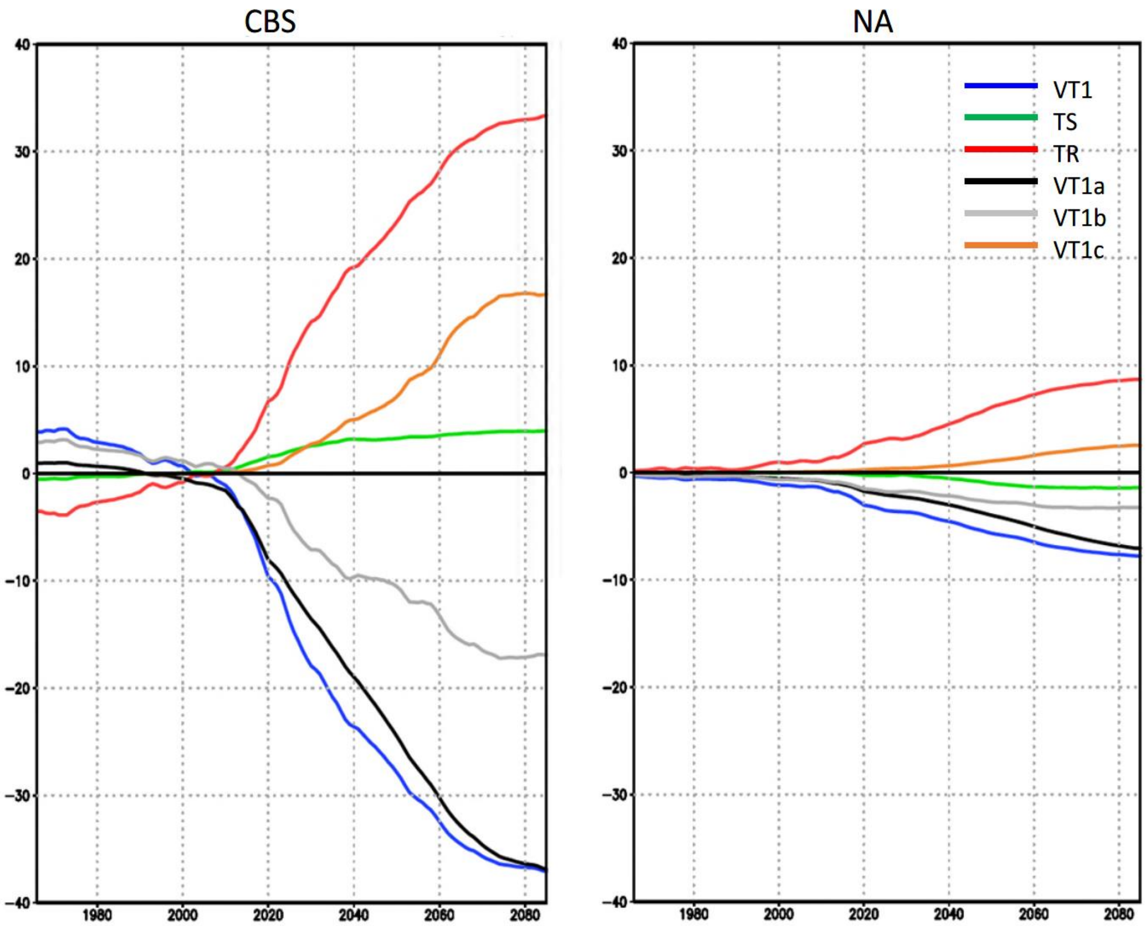

Figure 5 Reginal changes (in 10^{-6} $^oC^2s^{-1}$) of dominant terms VT1(blue), TS (green) and TR (red), as well as sub-components VT1a (black), VT1b (grey) and VT1c (orange) over 30-year running windows from 1951-2100 relative to the corresponding results over 1951-1980, averaged over the regions of (57.5-75^{o}N, 175^{o}E-150^{o}W) in CBS (left) and (45-65^{o}N, 120-75^{o}W) in NA (right) as shown in Fig. 2. Years are labeled based on year 15 of a 30-year window.